DOE/ER/14762-7

LOW ENERGY COLLISIONS OF ATOMIC AND MOLECULAR IONS

Final Technical Report
DE FG 02-97ER14762
for the period
February 28, 1997 - March 31, 2005

R. L. Champion
Department of Physics
College of William and Mary
Williamsburg, Virginia 23187-8795
(champion@physics.wm.edu)
(757) 221-3510

November, 2005

repared for the U. S. Department of Energy under contract DE FG 02-97ER14762

TABLE OF CONTENTS

1. Introduction

During the contract period, our experimental activities concentrated on ion-surface collision studies, gas phase collisions, the effects of adsorbates on field emission, and the origin of H_3O^+ in mass spectroscopy. In the area of ion-surface collisions we have measured sputtering yields for negative ions and electrons arising from collisions of ions and photons with a variety of metallic substrates upon which is known amount of adsorbate, which drastically alters the emission characteristics. Kinetic energy distributions of the ejected anions and electrons have also been determined. We have developed a theoretical model which, to a large degree, describes the process and elucidates the role of the adsorbate in the emission processes. In an additional experiment performed at the Synchrotron Radiation Center (Madison, WI) we have studied secondary negative ion emission initiated by UV photons; those results are compatible with the predictions of the above-mentioned model. In the category of gas-phase collisions, we reported work on proton transfer and ion-molecule reactions for reactants involving H_3^+ and D_3^+, measured absolute cross sections for a variety inelastic channels for reactants involving CH_4^+ and CF_4, and finally, measured electron detachment and decomposition cross sections for collisions of SF_6^- with N_2. Additionally, we reported absolute cross sections for various reactive collisions involving collisional decomposition of SF_6^- and the reactants CF_3^+ and CHF_3. The idea here was to use these measured cross sections to model and understand the salient features of the popular gaseous dielectric, SF_6 , and the etching discharge which utilizes CHF_3. A somewhat different set of experiments explored the role of adsorbates on the process of electron field emission and the nature and origin of the anomalous cation signal often seen at mass 19 amu in mass spectroscopy.

The laboratory collision energies for these experiments ranged from a few electron volts up to 500 eV. The goal of all the studies was to develop an understanding of the collisional dynamics and pathways for systems which are both intellectually interesting and of some potential importance to various areas of applied physics.

Very brief accounts of these activities will be given in this report in section 2. Detailed discussions of the experimental results and their analyses, published during the contract period, may be found in the articles listed in section 3, all of which may be found in peer-reviewed archival literature.

2. Brief reviews of work performed

A. Ion-surface collisions

We demonstrated that ion-induced secondary electron and negative ion emission from metallic substrates is dramatically enhanced if a monolayer or so of oxygen is allowed to accumulate on the substrate surface. Those experimental results were explained with a model that provides for the yields and kinetic energy distributions observed for both the electrons and anions. The model is characterized by the excitation of a substrate-adsorbate negative molecular ion (such as WO^- for a tungsten substrate) to an anti-bonding state. This electronically excited state may then decay via electron emission into the vacuum or alternately, the O^- may survive intact into the vacuum. We extended these types of measurements to include other adsorbates and the results for W/O are compared to those for W/Cl in

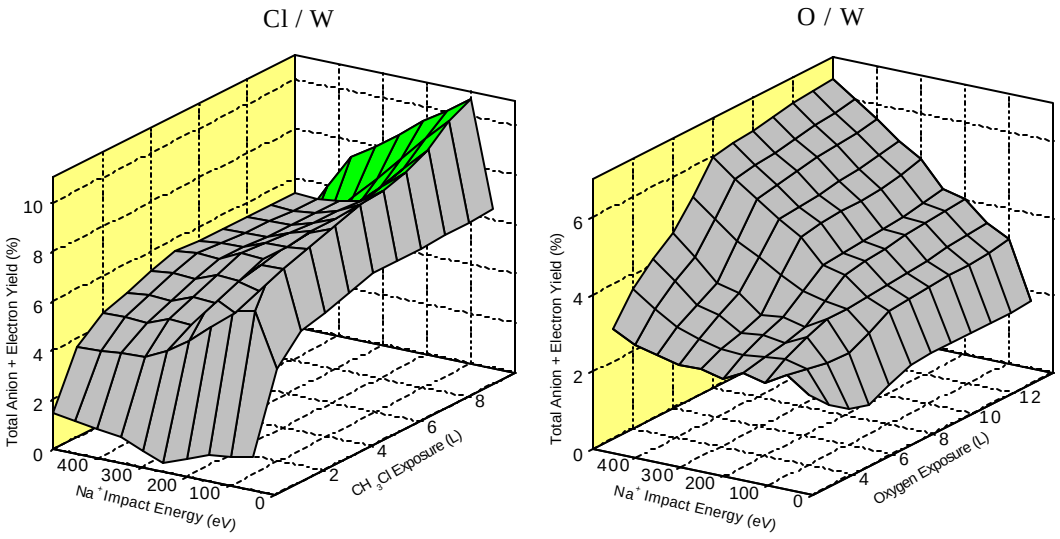

Figure 1 *The probabilities for ion-induced secondary anion and electron emission from tungsten as functions of both impact energy and coverage of Cl (left) and O (right) are shown as percentages.*

figure 1 in which the total negative ion and electron yields are shown as a function of (positive) ion impact energy and the amount of adsorbate on the surface. As may be seen in the figure, the two adsorbates dramatically enhance the secondary emission processes and do so in completely different ways. The goal of these experiments was to understand ion/atom -surface interactions for energies common to discharges used for materials processing and plasma containment devices. The experiments were performed for impact energies ranging from the energetic threshold observed for the processes (. 50 eV) up to 450 eV.

A1. Secondary Negative Ion and Electron Emission: Mo(100)/O

Absolute yields for secondary electron emission and O^- sputtering due to positive ion impact were determined for Mo(100) with a fractional coverage of adsorbed oxygen. Both the electron- and anion yields are essentially zero for no oxygen coverage and grow linearly with the coverage until it reaches about one monolayer. At moderate oxygen coverages, the yields are quite large for impact energies of a few hundred eV. Thus, anion and electron sputtering play an important role in discharge environments. Kinetic energy (K.E.) distributions of the sputtered oxygen negative ions and the secondary electrons were also measured. An example of these results is shown in figure 2 where electron and anion K.E. spectra are shown for 250 eV Na^+ striking Mo (100) with about 0.5 monolayer of adsorbed oxygen. Both processes were described with a model invoking the formation of a collisionally excited MoO^- surface state which subsequently dissociates producing electrons which (i) return to the metal, (ii) escape to the vacuum, or (iii) survive intact on the O^- as it

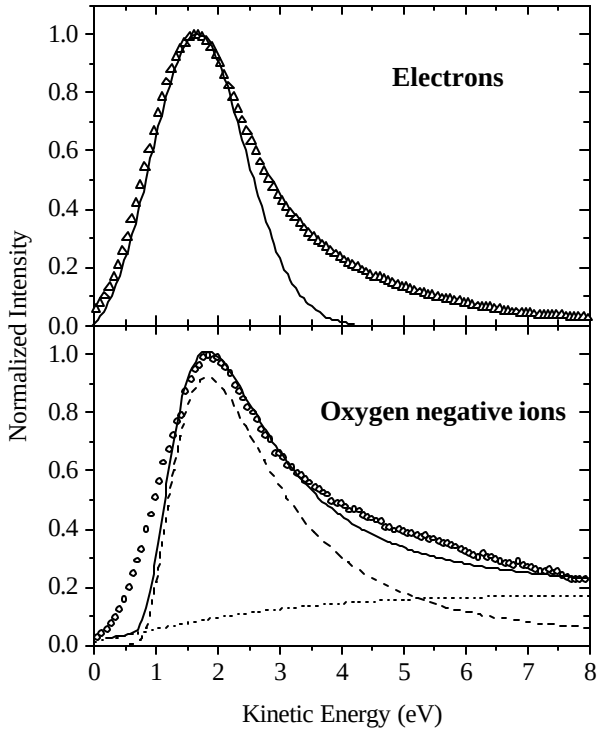

Figure 2. *The experimental kinetic energy distributions for electrons and O^- are shown as symbols. The lines are the results of calculations which utilize a model described briefly in the text.*

escapes into the vacuum. The electron K.E. distribution calculated with the model is shown as the solid line in the top panel of figure 2 and that for O^- as the dashed line in the lower panel. For the sputtered ions, an additional mechanism - a collision cascade, given by the dotted line - must be used to account for the high energy tail in the K.E. distribution for O^-. The net calculated K.E. distribution for the sputtered O^- is shown as the solid line in the lower panel of figure 2.

A2. Secondary negative ion and electron emission: photon-induced

The experimental results discussed above were explained with a model that could provide for the yields and kinetic energy distributions observed for both the electrons and anions. The model is similar in several respects to those used to describe desorption induced by electronic transitions (DIET) for other electron- and photon- stimulated surface processes and, in the present case, is characterized by the excitation of a substrate negative molecular ion (such as AlO^- for an Al substrate) to an anti-bonding state. Figure 3 shows a schematic representation of this process used to interpret the observations for the Al/O system. While this model was developed for ion impact, the mechanism for excitation should not, in principle, be limited to such. If the model is correct, one should observe the same characteristic secondary emission by direct excitation of the AlO^- surface state with photons of near-resonant energy.

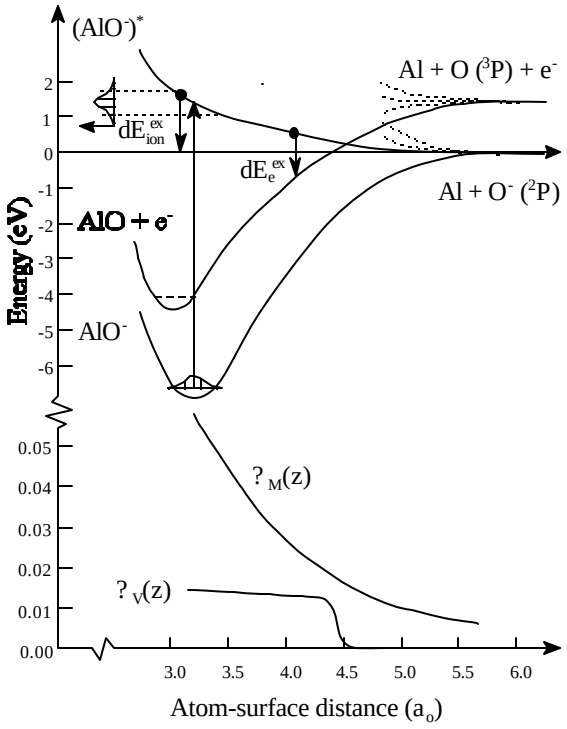

Figure 3 Schematic diagram of potentials used to describe ion-induced secondary emission of anions and electrons from an Al/O surface

A "proof of principle" experiment was carried out at the Synchrotron Radiation Center where the beamline was able to provide photons with energies ranging from 5 to 40 eV under UHV conditions. The experiments served two purposes, both to quantify the change in the surface work function as a result of oxygen coverage and, more importantly, to search for photon-induced anion emission as function of photon energy. The anion experiment was conceptually simple: An aluminum polycrystalline substrate was exposed to oxygen

and then to photons of a given energy. During the measurement the detector was biased to detect anions which left the Al/O surface with an energy of 2 ± 1.5 eV, corresponding to the most probable ion energy observed in the ion impact experiments. Figure 4 compares the anion emission from a clean surface (there is essentially none) to that from the same surface with about one monolayer of adsorbed oxygen. The photon energy required for maximum anion emission, 8.7 eV, is in remarkable agreement with the value required for a Frank-Condon transition between the AlO^- potentials illustrated in figure 3.

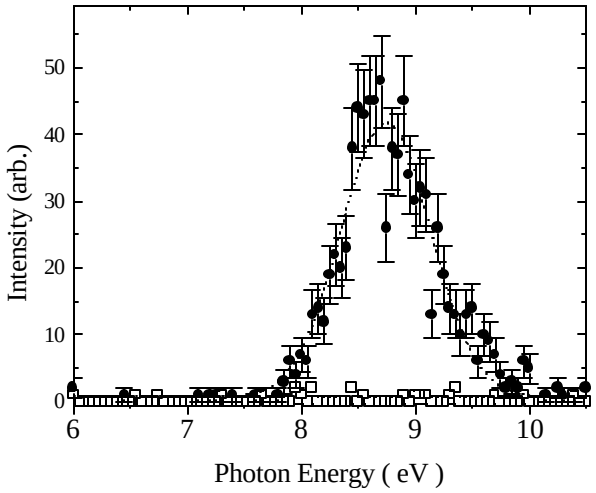

Figure 4 The yield for photon-induced anion emission is shown as a function of photon energy for an Al substrate with 1 ML adsorbed oxygen [Ž] and for clean Al [9].

A3. Secondary negative ion and electron emission: stainless steel.

Secondary electron and anion yields were measured for stainless steel surfaces with surface conditions ranging from those found in normal electrodes to a surface completely free of adsorbates. The motivation behind those experiments was to ascertain the (often time-dependent) role of discharge electrodes in determining the equilibrium concentrations of electrons and negative ions in various plasmas. The yields are shown in figure 5 as a function of ion impact energy for three surface conditions: a surface with no *in situ* cleaning- [squares], after heating to

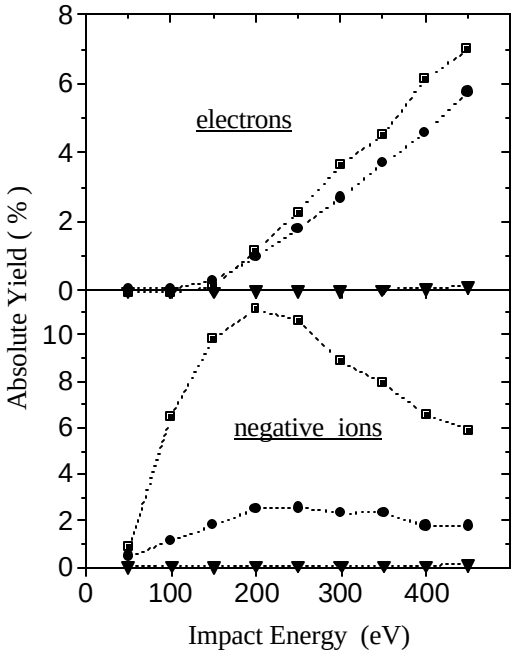

Figure 5 Secondary yields vs. impact energy for stainless steel with three surface conditions (see text).

600 °C -[circles], and after heating and sputter-cleaning - [triangles]. The secondary yields decrease dramatically as the surface becomes free of adsorbates, most of which was oxygen. We used these results to explain some of the observed properties of an oxygen discharge.

A4. Si(100) substrate.

The oxygen-chemisorbed silicon surface has been frequently explored owing to its connection to materials processing. The study of interactions of low-energy incident ions with these systems is related to understanding plasma interactions with the adsorbed silicon substrate, and sheds light on the nature of the chemisorption process as well. The detailed nature of oxygen adsorption to the many facets of silicon have been the subjects of numerous theoretical and experimental surface studies. In the case of Si(100), oxygen is thought to chemisorb both in its atomic and molecular form, with the former occurring in the initial stages of oxidation. In particular, it is thought that O_2 molecules initially adsorbed are unstable and dissociate as the surface topology of Si(100) relaxes back to that of a "perfect" surface. [The surface structure of clean Si(100) is not that of the perfect crystal. Every other pair of Si atoms on the surface moves closer together forming what is designated as a 2 x 1 surface topology. As oxygen is adsorbed on this 'reconstructed' surface, the espoused Si atoms move apart and the surface topology reverts to approximately that of the perfect crystal.] The oxygen atoms that adsorb do so essentially as O^- ; i.e., each adsorbed atom is calculated to gain 0.98 electrons from its neighboring silicon atoms. We performed an investigation on the effects of an oxygen adsorbate on secondary electron and anion emission. This emission was effected with positive sodium ions, having an impact energy in the range of 50 to 500 eV. The use of low energy positive sodium ions as a surface probe precluded secondary electron emission via kinetic (momentum transfer) and potential routes, the former since the impact energies were below 500 eV and the latter since the ionization potential of sodium is less than twice the work function for most metals, a necessary condition for Auger neutralization, which leads to potential emission.

The absolute probabilities for secondary emission of electrons and anions are shown in figure 6 as functions of the impact energy; the relative electron yield is seen to be quite small. In fact, the electron yield did not exceed 0.3% for any coverage or impact energy studied, in sharp contrast to what has been observed for metallic substrates. The anion spectrum arising from 250 eV Na^+ incident on the surface is shown in the inset of figure 6. The dominant peak is O^-, with a lesser contribution from

OH^-; peaks at 60 and 61 amu, due to SiO_2^- and SiO_2H^-, were also present.

The kinetic energy spectra for both O^- and e^- are independent of the sodium impact energy and oxygen coverage suggesting that the dynamics descriptive of secondary emission involve electronic excitation and not collisional momentum transfer. Moreover, electron kinetic energy spectra are very similar to those for the anions, suggesting that a common mechanism underlies emission of both. A model developed for ion-induced secondary emission from metallic substrates describes electronic excitation of a metal-adsorbate complex, e.g. MX^-, to a higher, repulsive potential, $(MX^-)^*$. This excitation can result in anion desorption into the vacuum, (M + X^-), or decay of the system to yield a free electron (M + X + e or MX + e). Several factors complicate this picture when applied to an adsorbed semiconductor substrate, the most important of which is the presence of a band gap and fairly tightly bound electrons in the valence band. An electron transfer mechanism which can occur on insulator or semiconductor surfaces involves Auger de-excitation. Here, an electron from the valence band transfers to an unoccupied orbital of an excited species located near or on the surface, and an electron is simultaneously emitted to the vacuum from the excited state. This process is often referred to as "Penning ionization" in collisions of highly excited metastable atoms with atoms or surfaces, where secondary electron emission is routinely observed. We suggest that secondary anion and electron emission follows impact-induced excitation of SiO^-. A schematic diagram of this process is shown in figure 7, including the positions of Si(100) surface states and the energy levels of Si(100). The subsequent decay of $(SiO^-)^*$ may result in O^- being ejected

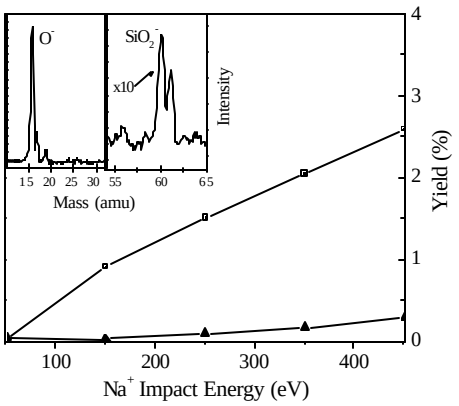

Figure 6 Secondary anion (squares) and electron (triangles) yields for Na^+ on Si(100) for an oxygen coverage of about 3/4 monolayer.

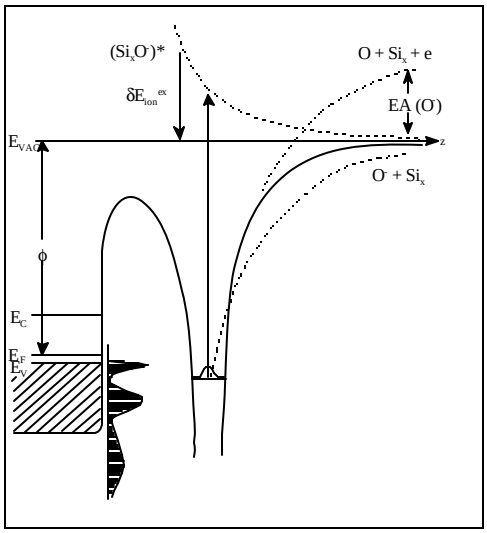

Figure 7 A schematic diagram illustrating the potentials descriptive of O^- and Si(100). E_C is the bottom of the conduction band, E_F the fermi level.

into the vacuum intact, i.e., as O^-. The probability that O^- survives such a dissociation depends on how rapidly O^- leaves the surface and can be substantial for metallic substrates, as shown in previous experiments. Alternately, electron emission to the vacuum from $(SiO^-)^*$ could occur via a mechanism similar to the Penning ionization process if an electron from the silicon valence band transfers to fill the unoccupied orbital of (SiO^-). The rate for such a transfer process depends primarily on the overlap of the silicon valence band orbitals with those of the unoccupied states of (SiO^-). The relatively small probability for electron emission suggests that this orbital overlap is indeed small, perhaps due to a reduced spatial distribution of the surface wavefunctions. Furthermore, as $(O^-)^*$ recedes from the surface the energy level of the unoccupied orbital rises above the top of the valence band, and such autodetaching electron transfer will not occur. Secondary anions and electrons which originate from the decay of $(SiO^-)^*$ will have asymptotic kinetic energies (with respect to the vacuum) which depend on the initial position of $(SiO^-)^*$ on the antibonding state curve, as illustrated in figure 7. The energy distributions for e^- and O^- would then be similar; this is, in fact, observed.

A5. Rare gas ion projectiles.

The first substrate/adsorbate investigated using rare gas projectiles was Al/O and the results were unexpected. Figure 8 illustrates the case for Ne^+ impacting a Al/O surface. The squares are the results for a clean surface and the circles (triangles) represent a coverage of about one-half (one) monolayer of oxygen on the Al substrate. The electron yield goes down as the coverage goes up, despite the fact that the macroscopic work function of the Al/O system *decreases* slightly with oxygen coverage in this range. Based upon previous experimental results where potential electron emission was precluded, one might expect that electron emission initiated by Ne^+ would be expressed as a sum of the auger-type potential emission and the adsorbate-related process described above.

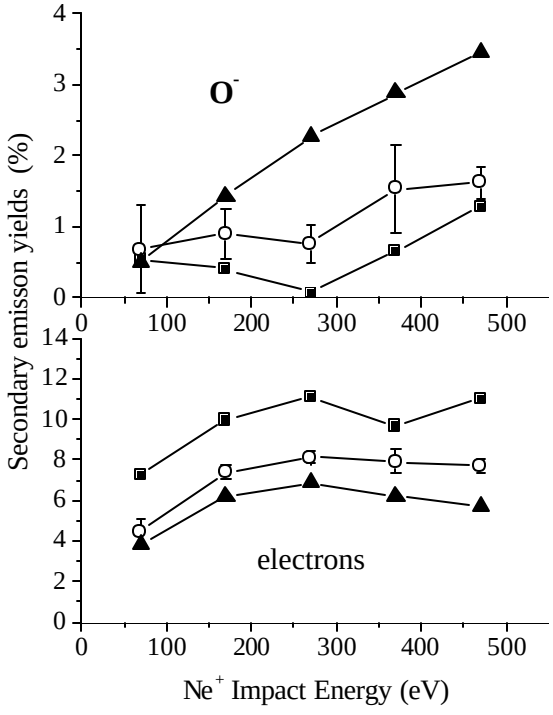

Figure 8 Secondary yields for Ne^+ on Al/O are shown for clean(•) Al; - ½ ml (•), and - one ml oxygen (•) on the substrate.

Clearly the situation is much more complicated. On the other hand the secondary yield for O^- is very similar in all respects to that initiated by ions with very low ionization potentials.

A6. Negative ion projectiles.

A series of experiments which used negative ions to initiate secondary emission from metallic substrates and the effects of adsorbates upon those processes was completed. One of the principal motivations for studying *negative-ion* - induced emission was to completely eliminate the role of potential energy (such as the recombination energy associated with the neutralization of an impacting positive ion) as a precursor for the secondary emission processes. An example of the results of these experiments is shown in figure 9 in which the probability of secondary electron emission is shown for O^- impacting a Cu(110) surface with various amounts of adsorbed oxygen. These observations are very similar to those observed for impacting alkali cations and support the notion that the underlying mechanism for adsorbate-altered secondary electron emission has essentially nothing to do with the recombination energy of the impacting particle. We have also measured the kinetic energy distributions of the secondary electrons (and secondary anions) and the results are consistent with our model developed for ion-induced, adsorbate-altered secondary emission.

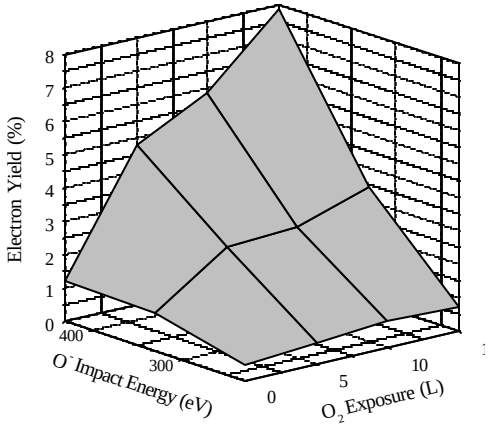

Figure 9 *The probability of secondary electron emission for O^- + Cu(110) is shown as a function of the O^- impact energy and adsorbed oxygen on the metallic substrate. (One monolayer of oxygen corresponds to an O_2 exposure of about 10 L.)*

A7. MgO: a metal-insulator transition. By exposing a pristine Mg crystal to oxygen it is possible to alter the substrate from metallic to approximately insulator conditions in a controlled manner. Exposing Mg(0001) to about 8 Langmuir (1 L = 10^{-6} torr-sec) of oxygen results in roughly one monolayer of oxygen adsorbed on the Mg surface. Subsequent exposure of the Mg to oxygen can result in an oxide build-up approximating that of a vapor-deposition grown Mg-oxide crystal. The latter is an insulator and, as such, has considerably different electronic properties near the surface. Our

goal in these experiments was to monitor the secondary emission properties as the oxide "grows" to ascertain if there are subsequent changes in the emission characteristics as the metallic/insulator transition occurs. Absolute secondary electron and anion emission probabilities for low energy (< 500 eV) O^-, N_2^+, Ar^+, Ne^+ and He^+ impacting an oxygen-adsorbed Mg(0001) single crystal surface were measured as a function of oxygen exposure and of incident ion impact energy. Secondary anion emission was observed throughout the range of adsorbate coverage studied, from that of a "clean" metal (defined by a demonstrated adsorbate-induced work function shift) to that rendering an insulative metal oxide, and was determined to comprise mostly O^-. Both electron and anion emission were observed to be largely unaltered as oxygen accumulated on the surface. Secondary anion and electron kinetic energy spectra were also measured; no significant dependence on oxygen exposure was observed The results for 270 eV Ar^+ impacting Mg are shown in figure 10. Aside from initial changes in the emission - undoubtedly related to the severe change in the surface work function upon initial oxidation - there is relatively little alteration in the electron emission as the oxidation progresses. Once again, this observation is compatible with the notion that the underlying mechanism for emission is similar to that described in the previous paragraphs.

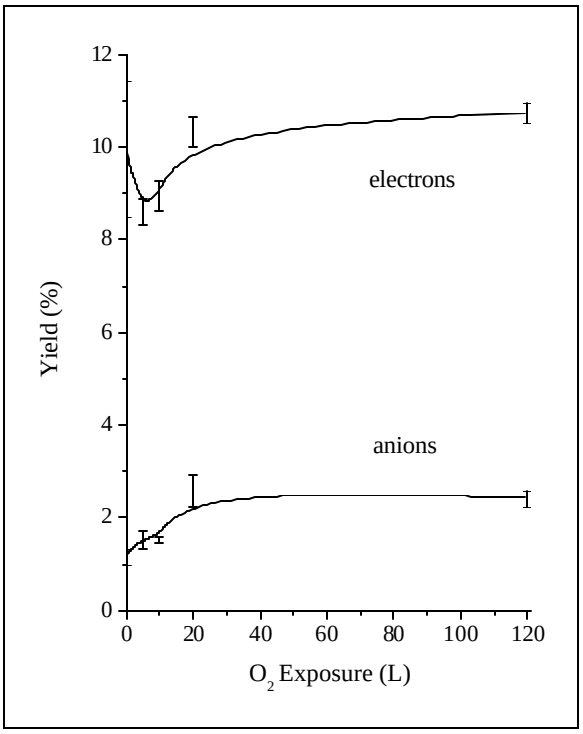

Figure 10 *The secondary yields of electrons and O^- which result from Ar^+ (270 eV) impacting Mg(0001) as a function of oxygen exposure are shown.*

B. Gas phase interactions

B1. Proton transfer and ion-molecule reactions with H_3^+

By using an experimental arrangement which employs both a static gas collision cell and a crossed-beam configuration, we measured absolute cross sections and product branching ratios for collisions of H_3^+ and D_3^+ with various atomic and molecular targets. For collisions of H_3^+ with H_2, proton transfer to the target (creating a "new" H_3^+ ion) exhibits a large cross section for relative collision energies below about 10 eV. These collisions often result in the formation of excited H_3^+ product ions, some of which subsequently autodissociate producing slow protons or H_2^+. The branching ratios for proton transfer and/or subsequent decomposition of the newly formed triatomic ion are shown in figure 11 for both $H_3^+ + H_2$ and $D_3^+ + D_2$. It is obvious that proton (deuteron) pick-up by the target is often sufficiently inelastic to cause the resulting triatomic product ion to dissociate into $H_2^+ + H$ or $H^+ + H_2$. These cross section measurements are essential input required to model and hence understand the equilibrium concentrations and ionic energy distributions in hydrogen discharges, where H_3^+ is routinely the dominant molecular ion. The species- and energy distribution-measurements have been made for a DC hydrogen discharge in a collaborative effort with a group at NIST. This work was directed toward achieving the goal of successfully modeling this simplest of molecular discharges, *viz.*, hydrogen.

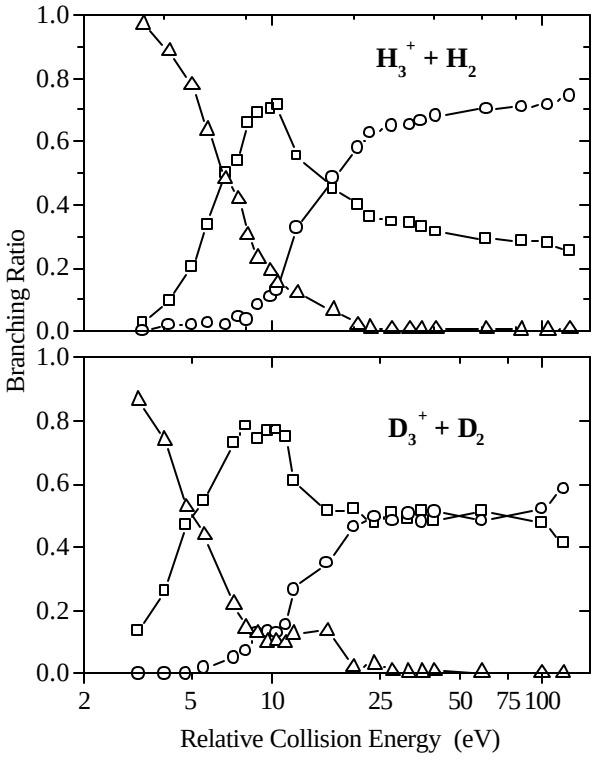

Figure 11. *The branching ratios for proton transfer*[?], *and the formation of slow* H^+[~] *and* H_2^+[O] *are shown for* $H_3^+ + H_2$ *and its isotopic equivalent. The* H^+ *and* H_2^+ *ions presumably arise from autodissociation of excited products,* $[H_3^+]^*$

B2. Inelastic collisions involving CH_4^+

Information required for modeling methane-containing discharges such as those used in CVD source plasmas are generally unavailable for collision energies common to such discharges. In an attempt to address that problem we have measured cross sections for proton and electron transfer and collision-induced dissociation for collisions of CH_4^+ with CH_4, H_2 and Ar. An example of the results for $CH_4^+ + CD_4$ is given in figure 12. Proton transfer, forming CD_4H^+ is exothermic by about 1 eV and its cross section rises as the collision energy falls below 10 eV. Notice that the CD_3^+ (indicated by the triangles in figure 12) can be formed in two distinct ways; either by dissociative proton transfer *to* the target or dissociative electron transfer *from* the target. The peak for CD_3^+ observed for E . 100 eV should be due to the latter and the peak at E . 10 eV is undoubtedly due to the former. Despite the obvious complications of these rather large systems, we made some progress in understanding their collisional dynamics.

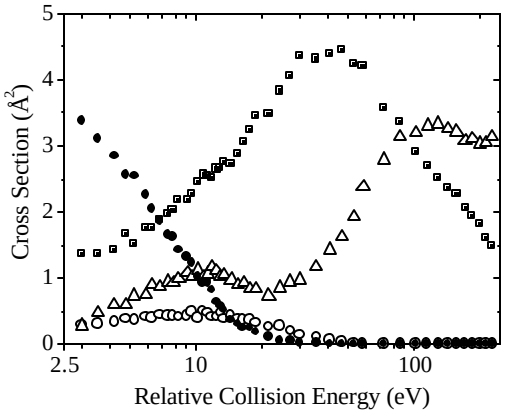

Figure 12 Cross sections for $CH_4^+ + CD_4$---proton transfer giving CD_4H^+ [Ž],and CD_2H^+[•];charge transfer giving CD_4^+[•]; and, finally, CD_3^+[?].

B3. Ion- Molecule Collisions with SF_6^-

Sulfur hexafluoride is an excellent dielectric gas, used throughout the world in high voltage switching and transmission equipment. Its dielectric qualities are due to its extraordinarily large cross section for electron attachment and its stability against electron detachment in subsequent collisions with SF_6. SF_6 is user-friendly in the lab, but it turns out that it can be a very potent greenhouse gas, owing to its long lifetime in the upper atmosphere (perhaps several thousand years). Unfortunately SF_6 seems to be routinely released into the atmosphere. One pseudo-fix which has been suggested is to replace SF_6 with 50-50 mixtures of SF_6 and N_2. Such a mixture can have about 75 - 80% of the dielectric strength of pure SF_6. Hence it is of interest to know the various cross sections for collisions of SF_6^-

with N_2. Accordingly, cross sections for electron detachment and collision-induced dissociation were measured for collisions of these reactants. The experiments were performed for collision energies ranging from a few up to several hundred electron volts.

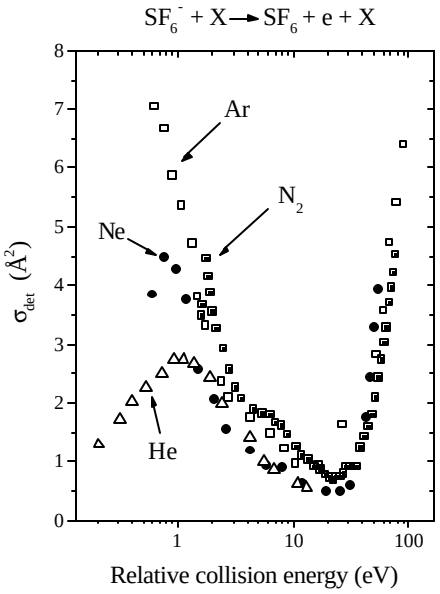

Figure 13 *The cross section for collisional electron detachment of SF_6^- is given for four targets.*

The cross section for electron detachment, $s_{det}(E)$, is given in figure 13 as a function of the relative collision energy, E, for the nitrogen target along with that for several rare gases. There are several striking things about the results. First, there isn't much difference in $s_{det}(E)$ for the various targets. Second, $s_{det}(E)$ has a peculiar shape with a minimum in the vicinity of E = 25 eV. The salient features of these observations and those for collision-induced dissociation (into either $SF_5^- + F$ *or* $SF_5 + F^-$) are roughly described with a two-step model in which collisional excitation of SF_6^- - which is an almost-universal function of the relative collision energy - is followed by unimolecular decomposition. The decomposition rates were calculated with a statistical phase space model with inputs from recent theoretical calculations for sulfur hexafluoride and its ions.

B4. Reactive collisions relevant to a CHF_3 discharge.

Trifluoromethane (CHF_3) is used in semiconductor plasma processing chambers to achieve high etch selectivity of an oxide layer over a silicon substrate. Such surface etching is governed by the ion and molecule fluxes near the surface, the concentrations of which are dependent upon species interactions in and their transport through the plasma. In order to assist in the interpretation of ion flux measurements and to provide fundamental data required for plasma modeling, we measured total cross sections for significant ion-molecule reactions occurring in CHF_3 discharges. The reactions studied included collision induced dissociation for CF_3^+ on CHF_3, dissociative charge transfer for CF_3^+ and F^+ on CHF_3, and electron detachment from F^- on CHF_3. Collision energies range from a few to a few

hundred electron volts. A myriad of ions and neutrals are formed from the reactants studied here; the results for collisions of F^+ with CHF_3 are shown in figure 14. A few general conclusions may be drawn from the experimental observations. Large cross sections for electron detachment, ~14 $Å^2$, dissociative charge transfer for ionized fluorine, ~25 $Å^2$, and collision induced dissociation, ~6 $Å^2$, indicate that neutral fluorine, one of the most important radicals in semiconductor etching, is a dominant species in CHF_3 discharge environments. The cross section for the production of the CF_3 radical is substantial as well, *viz*.~26 $Å^2$, for higher collision energies.

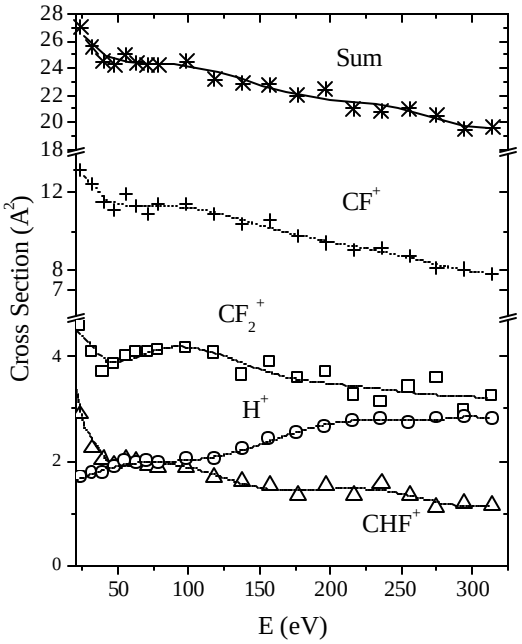

Figure 14 *Dissociative charge transfer cross sections for collisions of F^+ with CHF_3 are presented for four product channels as a function of relative collision energy.*

C. Field emission - the effects of adsorbates

One of our goals in studying field emission was to ascertain the role of adsorbates on both the intensity and energy distributions of the field emitted electrons. Field emission with a remarkably narrow energy distribution of 68 meV FWHM was observed from a thermally cleaned Mo<110> single tip; such a distribution is seen in figure 15.

The emission spectra were taken with the emitting surface at 295K, using a double-pass cylindrical mirror analyzer in ultra high vacuum. This narrow energy distribution is attributed to a nanotip spontaneously formed on the ~75 nm radius Mo tip from *in situ* buildup by field induced surface diffusion. Auger electron spectroscopy (AES) showed that residual surface Ca segregated from the bulk during thermal cleaning and is a probable source of mobile atoms that formed the nanotip. A close examination of figure 15 would show a discernible doublet in the peak distribution that is attributed to a variation in the localized density of states of the nanotip. Sub-Langmuir oxygen exposure of the Mo tip immediately increased the energy distribution more than an order of magnitude to a FWHM of >1 eV, as shown in figure 16. The magnitude of the emission sometimes increases upon adsorbate coverage, but not always. The schematic energy diagram given in figure 17 is designed to illustrate the potential that an electron can experience when an adsorbate atom is at a given distance - 10 a_o in the figure - from the surface.

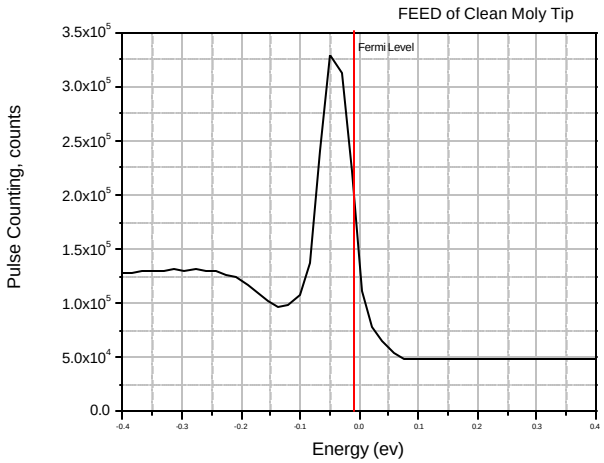

Figure 15 *Energy distribution for field-emitted electrons for a clean Mo tip.*

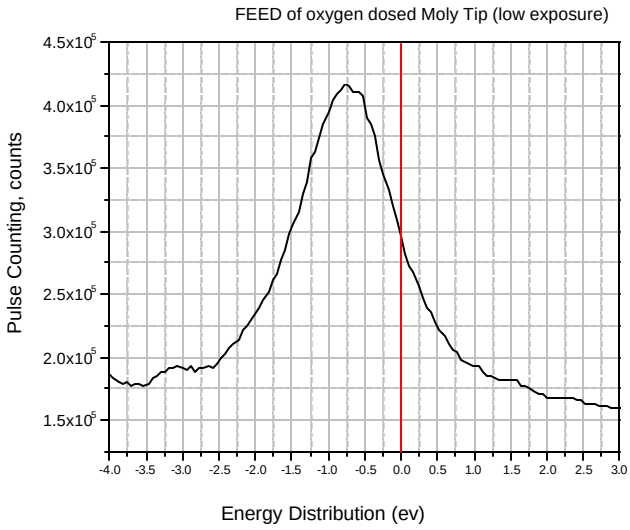

Figure 16. *Energy distribution after sub-monolayer exposure of Mo tip to oxygen*

In the absence of an adsorbed atom, field emission can occur for strong fields (on the order of a few tenths of a volt per atomic unit of distance) when metal electrons near the fermi level tunnel through or pass over the Schottky barrier indicated by "surface + field" in the figure. By having an adsorbate atom positioned near the surface the metal electron can see a lowered barrier and, in fact, an intermediate, unoccupied, quasi-bound state which separates it from the vacuum. Such a potential is shown as "surface + atom + field" in the figure and is typical for an oxygen adsorbate. It is obvious that field emission can be enhanced by the presence of the atom. At the close of this project, much remained to be learned about relationship of the surface to field emission characteristics.

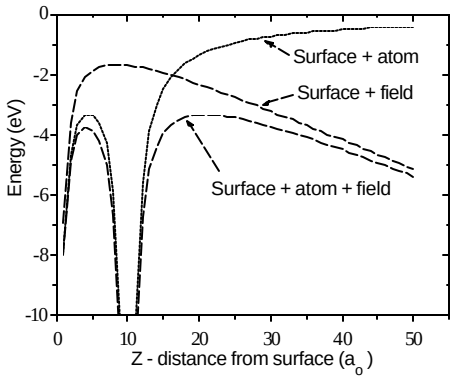

Figure 17 *A schematic diagram of the potential "seen" by an electron within the metal.*

D. Hydronium ion formation in FTMS

Typically, the mass spectral peak observed at 19 amu in residual gas analyzers at very high (VHV) and ultrahigh vacuum (UHV) has been attributed to fluorine. Using Fourier Transform Mass Spectrometry (FTMS), the presence of the hydronium ion, H_3O^+, was fully resolved from F^+. Correlation of the mass 19 signals for a conventional quadrupole mass spectrometer (QMS) and the FTMS, positioned adjacent, unambiguously indicates hydronium as the source of mass 19. At partial pressures of H_2O in the VHV range and higher there is sufficient density for the formation of the hydronium ion through ion-molecule interactions. Formation of the hydronium was found to directly correlate with the partial pressure of H_2O. However, in a QMS, formation of H_3O^+ in UHV appears to occur principally by electron stimulated desorption (ESD). Dosing the system with hydrogen from 1 Langmuir exposure to saturation (1×10^{-6} Torr for 8 hours) was found to increase the H_3O^+ ESD yield detected by the QMS by as much as a factor of 10. The initial hydronium ESD cross section from a hydrogen saturated grid was estimated to be $\sigma \sim 1 \times 10^{-19}$ cm^2. In a separate experiment, TOF-SIMS sputter yields from the stainless steel grid of a quadrupole mass spectrometer also showed small signals of H_3O^+, as well as its constituents, H^+, O^+ and OH^+, but no F^+.

Subsequent work was done to show that ESD of hydronium ions from stainless steel (such as

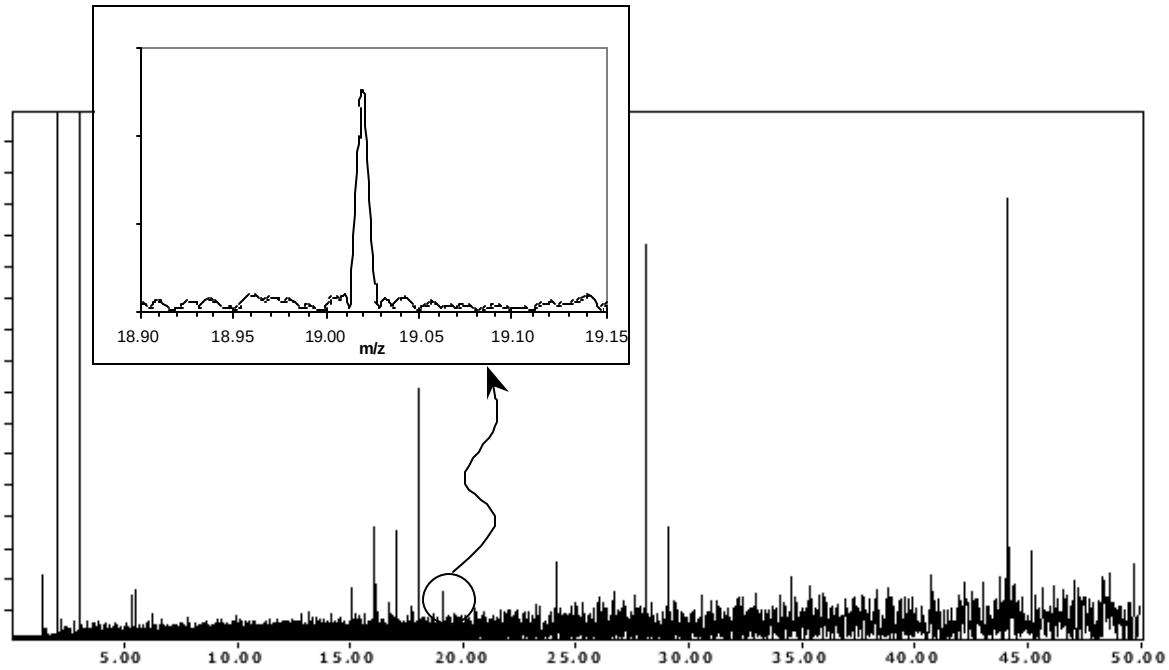

Figure 18 *Standard QMS mass spectra over 0 – 50 amu. The inset - a high resolution FTMS mass spectrum - shows that the signal is unambiguously H_3O^+, with a mass of 19.02 amu.*

constitute the grids and other surfaces in a conventional mass spectrometer) readily occurred. Hence the source of H_3O^+ in a conventional QMS is identified.

3. Publications in technical journals during the contract period.

Total cross sections for low energy collisions of H_3^+ with molecular hydrogen and rare gases

B. L. Peko and R. L. Champion
J. Chem. Phys.**107** , 1156 (1997).

On the dynamics of secondary-electron and anion emission from an Al/O surface.
J. C. Tucek and R. L. Champion
Surf. Sci. **382**, 137 (1997).

Ion-induced secondary electron and negative ion emission from Mo/O.
J. C. Tucek, S. G. Walton, and R. L. Champion
Surf. Sci. **410**. 258 (1998).

Negative ion emission from a stainless steel surface due to positive ion collisions.
S. G. Walton, R. L. Champion, and Yicheng Wang
J. Appl. Phys. **84,** 1706 (1998).

Collision-induced dissociation, proton abstraction, and charge transfer for low energy collisions involving CH_4^+.
B. L. Peko, I. V. Dyakov, and R. L. Champion
J. Chem Phys. **109**, 5269 (1998).

Photon-Induced anion emission: A mechanism for ion-induced secondary-electron emission from an Al/O surface.
S. G. Walton, B. L. Peko, and R. L. Champion
Phys. Rev. **B58**, 15430 (1998).

Cross section measurements for various reactions occurring in CF_4 and CHF_3 discharges.
B. L. Peko, I. V. Dyakov, and R. L. Champion
Gaseous Dielectrics VIII , ed by L. Christophorou and J. Olthoff. Plenum Press New York, 1998, p 45 ff.

Low energy, ion-induced electron and ion emission from stainless steel: The effect of oxygen coverage and the implications for discharge modeling.
S. G. Walton, J. C. Tucek , R. L. Champion and Y Wang.
Journal of Applied Physics **85**, 1832 (1999).

Ion-molecule reactions and ion energies in a CF_4 discharge.
B. L. Peko, I. V. Dyakov, R. L. Champion, M.V. Rao and J. K. Olthoff.

Phys. Rev **E60**, 7449 (1999).

The role of O and Cl adsorbates on the secondary emission properties of tungsten.
W. S. Vogan, S. G. Walton and R. L. Champion
Surface Science **459**, 14 (2000).

Collisional decomposition of the sulfur hexafluoride anion (SF_6^-)
R. L. Champion, I.V. Dyakov, B.L. Peko, and Y. Wang
Journal of Chemical Physics **115**, 1765 (2001).

Oxygen adsorption on a Si(100) substrate: Effects on secondary emission properties
W.S. Vogan and R.L. Champion
Surface Science **492,** 83 (2001).

Measured cross sections and ion energies for a CHF_3 discharge
B. L. Peko, R. L. Champion, M. V. V. S. Rao and J. K. Olthoff
Journal of Applied Physics **92**, 1657 (2002).

Mass spectral resolution of F^+ and H_3O^+ in very high vacuum.
C. R. Cole, B. C. Holloway, R. A. Outlaw, R. L. Champion and D. H. Baker
Jour. Vac. Sci. & Tech. **A21**, 1796 (2003).

The role of an oxygen adsorbate on the secondary emission properties of low energy ion-bombarded magnesium
W. S. Vogan, R. L. Champion and V. A. Esaulov
Surface Science **538**, 211 (2003).

Contribution and origin of H_3O^+ in the mass spectral peak at 19 amu
C. R. Cole, R. A. Outlaw, R. L. Champion, D. H. Baker, and B. C. Holloway
J. Vac. Sci. Technol. **A 22**, 2056 (2004).

Field emission from a Ca nanotip grown on a Mo microtip
Xin Zhao, R. A. Outlaw, R. L. Champion, J. J. Wang, D. M. Manos, and B. C. Holloway
Appl. Phys. Lett. **85,** 1415 (2004)